

Measurement of Kaon Directed Flow in Au+Au Collisions in the High Baryon Density Region

The STAR Collaboration

(Dated: April 1, 2025)

Rapidity-odd directed flow v_1 measurements are presented for K^\pm and K_S^0 in Au + Au collisions at $\sqrt{s_{NN}} = 3.0, 3.2, 3.5$, and 3.9 GeV with the STAR experiment. For comparison, v_1 of π^\pm , protons, and Λ from the same collisions are also discussed. The mid-rapidity v_1 slope $dv_1/dy|_{y=0}$ for protons and Λ is positive in these collisions. On the other hand, v_1 slope of kaons exhibits a strong p_T dependence: negative at $p_T < 0.6$ GeV/ c and positive at higher p_T . A similar p_T dependence is also evident for the v_1 slope of charged pions. Compared to the spectator-removed calculations in Au+Au collisions at $\sqrt{s_{NN}} = 3.0$ – 3.9 GeV, the JAM model demonstrates a pronounced shift of the v_1 slopes of mesons towards the negative direction. It suggests that the shadowing effect of the spectators plays an important role in the observed kaon anti-flow at low p_T in the high baryon density region of non-central collisions.

The goal of the Beam Energy Scan (BES) program at the Relativistic Heavy Ion Collider (RHIC) is to study the phase diagram of nuclear matter, which is governed by Quantum Chromodynamics (QCD) over a wide range of temperature and baryon density [1]. In the BES program, a Fixed Target (FXT) mode, implemented at the Solenoidal Tracker at RHIC (STAR), extends the coverage to the high baryon density region, the corresponding baryonic chemical potential $\mu_B \approx 720$ MeV, allowing a much wider region to be studied in the QCD phase diagram [2, 3]. In the high baryon density region, at collision energies of $\sqrt{s_{NN}} \lesssim 10$ GeV where hadronic interactions dominate [4], strange hadrons (e.g., kaons) produced via associate production, $N + N \rightarrow K + \Lambda + N$, serve as sensitive probes for the Equation of State (EoS) of the medium [5, 6]. Studying the nature of the interactions, particularly those which involve strange particles, is important for understanding the collision dynamics and extracting the EoS information in heavy-ion collisions and compact stars [7–10]. Driven by the early pressure gradient, the anisotropic flow of strange hadrons provides an ideal tool for studying the QCD phase structure.

The directed flow v_1 is the first harmonic coefficient of the Fourier expansion of the azimuthal distribution of emitted particles with respect to the reaction plane [11]. The rapidity-even v_1 is attributed to fluctuations in the initial geometry [12, 13]. The rapidity-odd v_1 investigated in this paper reflects the collective sideward deflection of the particles. It is also sensitive to the medium properties at the early stage of heavy-ion collisions [14–20], and can reveal the interplay between initial compression and tilted expansion [21, 22]. Early hydrodynamic calculations [23, 24] with first order phase transition have predicted a minimum of net-baryon’s mid-rapidity v_1 slope ($dv_1/dy|_{y=0}$) as the softest point of the EoS. This minimum is an indication of the phase transition between Quark Gluon Plasma (QGP) and hadronic phases [25, 26], but no calculation has yet predicted its location [24, 27–29]. In the high baryon density region of heavy-ion collisions, the passage time of the projec-

tile and target spectators is comparable to the dynamic evolution time [30–33]. The presence of spectators influences the collision dynamics due to interactions between the produced hadrons and the spectators [34–37]. Negative elliptic flow has been observed for all particles in collisions at $\sqrt{s_{NN}} < 3.5$ GeV [4, 34, 38], and can be attributed to the shadowing effect caused by the spectators. Transport model calculations indicate that the spectator shadowing effect is responsible for the negative v_1 slopes, also known as anti-flow, observed for pions and nucleons [31, 37, 39].

More than two decades ago, measurements from the E895 experiment at BNL-AGS revealed that K_S^0 with a relatively small scattering cross-section ($\sigma_{K^0-p} \sim 10$ mb) exhibits anti-flow within $p_T < 0.7$ GeV/ c in Au + Au collisions at $\sqrt{s_{NN}} = 3.83$ GeV [35]. This was explained by incorporating a repulsive kaon potential in nuclear collision model at high baryon density regions [40–46]. However, STAR measurements show positive v_1 slopes of kaons within $0.4 < p_T < 1.6$ GeV/ c in Au + Au collisions at $\sqrt{s_{NN}} = 3.0$ GeV [4]. Therefore, it is imperative to conduct systematic measurements of the collision energy, rapidity (y), and transverse momentum (p_T) dependence of directed flow for a variety of hadrons in high baryon density regions. This is essential for understanding the anti-flow of kaons and, more importantly, for gaining insight into kaon-nucleon interactions and the EoS including strange quark hadrons.

We report measurements of v_1 for π^\pm , K^\pm , K_S^0 , protons, and Λ in Au + Au collisions at $\sqrt{s_{NN}} = 3.0, 3.2, 3.5$, and 3.9 GeV. These data were recorded in 2018, 2019, and 2020 from the STAR FXT mode at RHIC. We require the primary vertex position along the beam direction (V_z) to be within 2 cm of the center of the target [4], which is located at ~ 200 cm from the center of Time Projection Chamber (TPC) [47, 48]. Additionally, the primary vertex position must be within a radius of less than 1.5 cm in transverse direction from the nominal primary vertex, which is ~ 2 cm below the nominal beamline, to exclude events from the vacuum

beam pipe. For charged particle tracking, the TPC is used at $\sqrt{s_{NN}} = 3.0$ GeV within the pseudorapidity (η) range $-2.0 < \eta < 0$ in the lab frame. The TPC and upgraded inner TPC (iTPC) are used at $\sqrt{s_{NN}} = 3.2, 3.5$, and 3.9 GeV within $-2.4 < \eta < 0$. Tracks are required to have a distance of closest approach (DCA) to the primary vertex of less than 3 cm and at least 15 space points for track reconstruction in the TPC. Collision centrality is determined by the number of charged tracks detected with the TPC and iTPC within the pseudorapidity (η) range $-2.0 < \eta < 0$ or $-2.4 < \eta < 0$, which is corroborated with simulations using the Monte Carlo Glauber model [49].

For the identification of π^\pm , K^\pm , and proton, a combination of TPC and Time Of Flight (TOF) [48, 50] detectors is used. The TPC provides ionization energy loss information, while the TOF provides time-of-flight information, which ensures that the purity of π^\pm and proton are greater than 95%, and the purity of K^\pm is greater 90%. The Kalman Filter (KF) particle package [51] is used to reconstruct weak decay particles, such as K_S^0 and Λ . In this process, the covariance matrix of reconstructed tracks is used to construct a set of topological variables. The particle density distribution as a function of rapidity y and transverse momentum p_T is shown in Fig. 1 for π^+ , K^+ , K^- , and K_S^0 , which are measured in Au + Au collisions at $\sqrt{s_{NN}} = 3.0, 3.2, 3.5$, and 3.9 GeV. The rapidities are presented in the center-of-mass frame, where the target is located at $y \approx -1$, indicated by the red arrows in the top panels of Fig. 1. The identified particles are required to be in the transverse momentum range of $0.2 < p_T < 1.6$ GeV/c for π^+ , $0.4 < p_T < 1.6$ GeV/c for K^+ , K^- , and K_S^0 , and the rapidity range is required to be within $-1 < y < 0$. Note that endcap TOF (eTOF) [52] is used at $\sqrt{s_{NN}} = 3.5$ and 3.9 GeV to extend the coverage, but leaves a small gap due to lack of overlap with barrel TOF (bTOF).

The reaction plane is estimated using the event plane method [11]. The Event Plane Detector (EPD) [53] is used for event plane determination within $-5.3 < \eta < -2.6$. In the STAR FXT mode, obtaining sub-events with equal particle multiplicity is not feasible. Due to the inequality of the sub-events, the event plane resolution obtained by the two sub-events method in each window can be different. Therefore, three sub-events are needed to determine the event plane resolution, which can be expressed as [11]:

$$R_1 = \langle \cos(\Psi_1^a - \Psi_r) \rangle = \sqrt{\frac{\langle \cos(\Psi_1^a - \Psi_1^b) \rangle \langle \cos(\Psi_1^a - \Psi_1^c) \rangle}{\langle \cos(\Psi_1^b - \Psi_1^c) \rangle}}, \quad (1)$$

where Ψ_r is the reaction plane angle, Ψ_1^a is the required event plane angle, and Ψ_1^b and Ψ_1^c are the reference event plane angles. We divide the EPD and TPC into three and two η windows, respectively. We choose the most

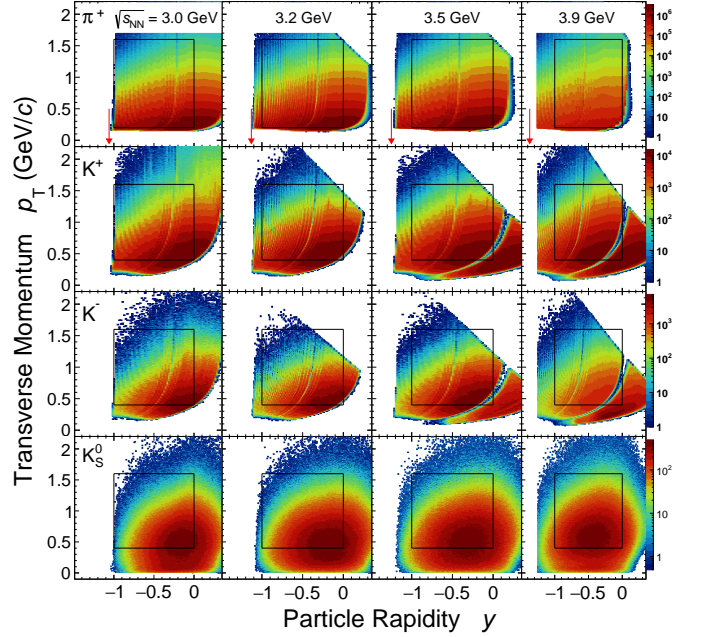


FIG. 1. The efficiency-uncorrected particle density distribution in transverse momentum and particle rapidity for π^+ , K^+ , K^- , and K_S^0 measured with STAR detectors TPC and TOF in Au + Au collisions at $\sqrt{s_{NN}} = 3.0, 3.2, 3.5$, and 3.9 GeV. Note that the red arrows show the target rapidity in the center-of-mass frame, and the black box exhibits the measured $p_T - y$ window.

forward η window ($-5.3 < \eta < -3.3$) in the EPD as the required event plane, while the other two reference event planes are taken from the next forward η window ($-2.9 < \eta < -3.0$) in the EPD and the most backward η window ($-1.15 < \eta < 0$) in the TPC. The directed flow can then be calculated by $v_1 = \langle \cos[(\phi - \Psi_1)] \rangle / R_1$, where R_1 is the resolution obtained above [11]. The first-order event plane resolutions in mid-central (10-40%) Au+Au collisions range from approximately 0.75 to 0.65 at $\sqrt{s_{NN}} = 3.0, 3.2, 3.5$, and 3.9 GeV. And the final results are corrected with event plane resolution, tracking efficiency and detector acceptance [26].

Systematic uncertainties in $v_1(y)$ and the mid-rapidity v_1 slope $dv_1/dy|_{y=0}$ are estimated by varying the track quality cuts, particle identification cuts, and choosing different reference event plane to determine event plane resolution. Specifically, the dominant contribution to the systematic uncertainty arises from the event plane resolution. For example, the systematic uncertainty from resolution is estimated to contribute 2.5% to the $dv_1/dy|_{y=0}$ measurement of protons in mid-central (10-40%) Au+Au collisions at $\sqrt{s_{NN}} = 3.5$ GeV. And the systematic uncertainty from track quality is determined by varying the DCA, is estimated to contribute 2.1%. The total systematic uncertainty is obtained by adding all uncertainties in quadrature, assuming the sources are uncorrelated.

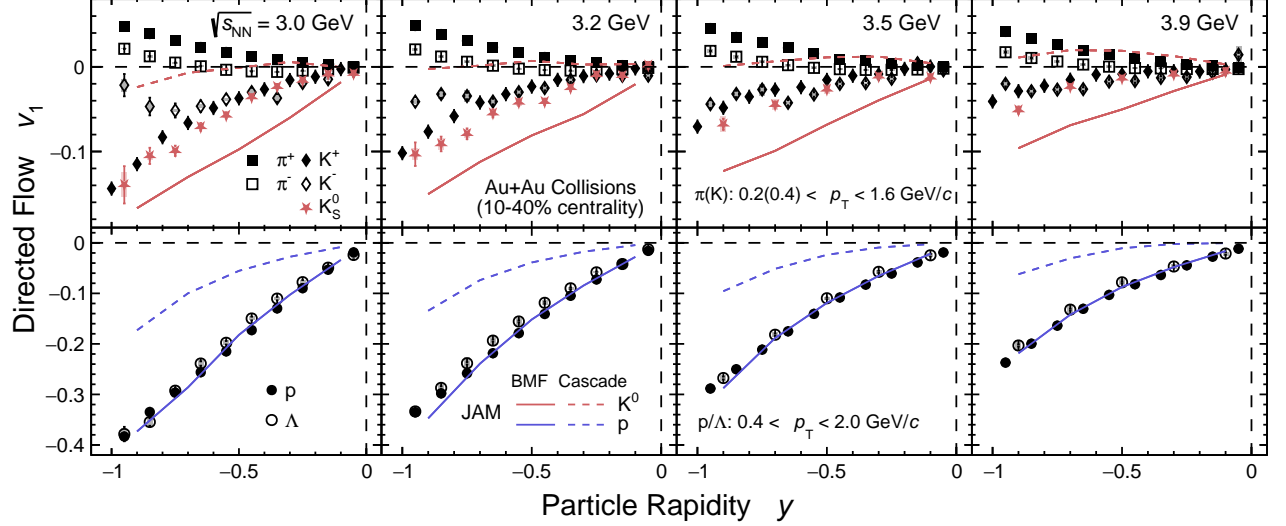


FIG. 2. Directed flow (v_1) of π^+ (solid square), π^- (open square), K^+ (solid diamond), K^- (open diamond), K_S^0 (solid star), protons (solid circle), and Λ (open circle) as a function of rapidity in mid-central (10-40%) Au + Au collisions at $\sqrt{s_{NN}} = 3.0, 3.2, 3.5$, and 3.9 GeV. Statistical and systematic uncertainties are shown as bars and gray bands, respectively. Data points of K^+ are shifted horizontally to improve visibility. The JAM calculations for K^0 and protons are represented by red and blue lines, with the dashed and solid lines representing cascade and baryonic mean-field (BMF) modes, respectively.

In Fig. 2, the v_1 of identified hadrons: π^\pm , K^\pm , and K_S^0 (top panels) and protons and Λ (bottom panels), are presented as a function of rapidity in mid-central (10-40%) Au + Au collisions at $\sqrt{s_{NN}} = 3.0, 3.2, 3.5$, and 3.9 GeV. The results are shown within the rapidity region $-1 < y < 0$ for all particles, and the corresponding p_T range for each hadron is indicated in the figure. The data at $\sqrt{s_{NN}} = 3$ GeV are from Ref. [4]. As depicted in the figure, the v_1 of pions is mostly positive, except for π^- at rapidity from -0.5 to 0, while the values of v_1 for kaons, protons, and Λ are all negative. Charged kaons and neutral kaons exhibit differences at forward rapidity, likely due to the Coulomb effect and the transported quark effect [54–58]. Additionally, the magnitude of v_1 exhibits a positive correlation with the mass of the hadron, i.e., hadrons with heavier masses tend to have larger values of v_1 . As collision energy increases, the v_1 magnitude of all particles are reduced. For comparison, the JET AA Microscopic Transport Model (JAM) [22, 59, 60] is used to compare with the experimental data, where particle production includes resonance excitation, string production, and their decay contributions, similar to other transport models such as RQMD, AMPT, and PHSD [61–64]. The collision centrality and p_T interval applied in the model calculations are the same as those in the data. And two different approaches are used to describe the effect of the EoS in JAM. One is the cascade method based on the modified two-body scattering [65], while the other involves the nuclear mean-field method implemented with the relativistic quantum molecular dynamic approach [66]. In the calculations involving baryonic

mean field interactions (mean-field), a nucleon incompressibility value of $\kappa = 210$ MeV is utilized, along with the incorporation of a momentum-dependent potential. It is evident that the model with the mean-field option accurately reproduces the rapidity dependence for protons, as shown by the solid blue lines in the figure. On the other hand, JAM in cascade mode (red dashed line) underestimates the v_1 of K_S^0 at $\sqrt{s_{NN}} = 3.0, 3.2, 3.5$, and 3.9 GeV, whereas JAM in mean-field mode (red solid line) overestimates the magnitude of v_1 . Note that the mean-field mode in transport models like JAM [22, 60] and UrQMD [67, 68] is specific to baryons, while the mean-field effect on mesons arises from the resonances in the model calculations, which are of the second order.

To quantify the strength of v_1 at the mid-rapidity, the rapidity distributions are fitted with a third-order polynomial function: $v_1(y) = Fy + F_3y^3$ within the rapidity range of $[-1, 0]$. The energy dependence of the mid-rapidity p_T integrated v_1 slope, $dv_1/dy|_{y=0}$, is characterized by the linear term F and shown in Fig. 3. The integrated v_1 slopes measured over the p_T range of 0.4 – 1.6 GeV/c are positive for kaons. This does not contradict the E895 observations, as the p_T ranges are different, and it implies that kaon anti-flow depends on the p_T ranges, which will be discussed later in detail. As energy increases, the values of $dv_1/dy|_{y=0}$ decrease for all particles, implying a reduction in mid-rapidity directed flow in higher energy collisions. In the high baryon density region, Λ are mostly produced via associative production, so Λ flow is similar to that of proton. As seen, the JAM model calculations with the baryonic mean-field re-

produce the energy dependence of the mid-rapidity p_T -integrated v_1 slopes for protons and Λ well. Note that JAM in cascade mode, which is not shown in the figure for clarity, exhibits v_1 slopes that are lower by a factor of four. The importance of the baryonic mean-field in baryon collectivity has also been observed in the flow measurements of v_2 for protons, Λ , light nuclei, and hypernuclei in Au+Au collisions at $\sqrt{s_{NN}} = 3.0$ GeV [4, 69, 70].

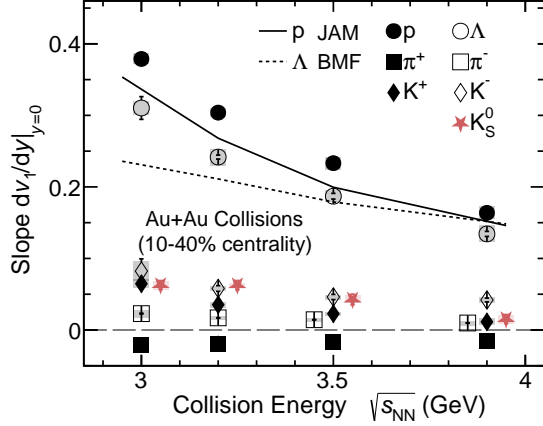


FIG. 3. Collision energy dependence of the p_T integrated mid-rapidity v_1 slope $dv_1/dy|_{y=0}$ for π^\pm , K^\pm , K_S^0 , protons, and Λ in mid-central (10-40%) Au + Au collisions. Statistical and systematic uncertainties are shown as bars and gray bands, respectively. Data points of π^- and K_S^0 are staggered by ± 0.05 GeV horizontally to improve visibility. The JAM calculations with baryon mean field for protons and Λ are shown as solid and dashed lines, respectively. The p_T ranges for pions, kaons, and protons/ Λ are $0.2 < p_T < 1.6$ GeV/c, $0.4 < p_T < 1.6$ GeV/c, and $0.4 < p_T < 2.0$ GeV/c, respectively.

At higher collision energies, $\sqrt{s_{NN}} \gtrsim 10$ GeV, the tilted expansion [21, 31, 71] dominates over initial compression, leading to the anti-flow of produced hadrons. In contrast, at lower energies, the interplay between initial compression and the strong shadowing effect from spectators and participant nucleons can also give rise to anti-flow [31, 37].

Figure 4 depicts results from systematic measurements of v_1 slopes for π^+ (solid circle), K^+ (solid diamond), K^- (open diamond), and K_S^0 (solid star) as a function of p_T in mid-central Au + Au collisions at $\sqrt{s_{NN}} = 3.0, 3.2, 3.5$, and 3.9 GeV. There is a strong p_T dependence for the v_1 slopes of both π^+ and kaons. Low- p_T ($p_T < 0.6$ GeV/c) anti-flow is observed for the measured mesons at all collision energies, while in the broader p_T range shown in Fig. 3, the p_T -integrated v_1 slope is positive. Additionally, the p_T dependence of the v_1 slopes is most pronounced at the lowest collision energy, $\sqrt{s_{NN}} = 3.0$

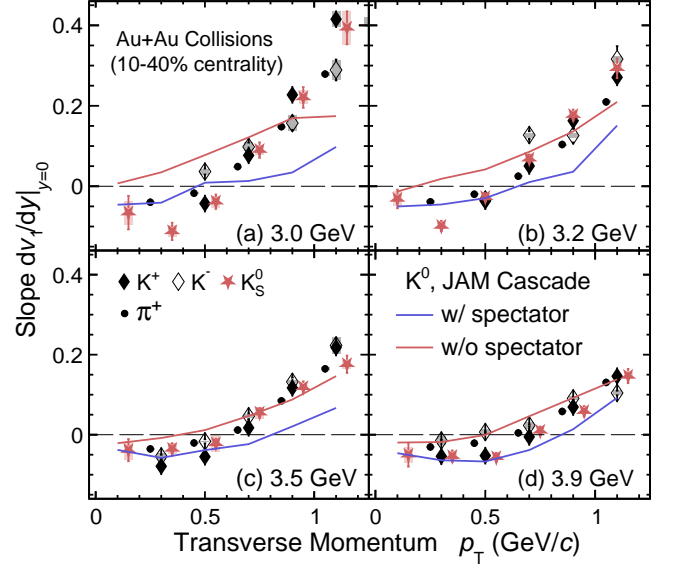


FIG. 4. Transverse momentum dependence of the mid-rapidity v_1 slope $dv_1/dy|_{y=0}$ for π^+ , K^+ , K^- , and K_S^0 in mid-central (10-40%) Au + Au collisions at $\sqrt{s_{NN}} = 3.0, 3.2, 3.5$, and 3.9 GeV. Statistical and systematic uncertainties are shown as bars and gray bands, respectively. Data points of π^+ and K_S^0 are shifted ± 0.05 GeV/c horizontally for better visibility. The JAM model calculations of $dv_1/dy|_{y=0}$ for K^0 : with and without the spectators are shown as blue and red solid lines, respectively. Note that $dv_1/dy|_{y=0}$ of K^\pm at $p_T < 0.4$ GeV/c are not measured for 3.0 and 3.2 GeV due to the limited acceptance.

GeV. STAR measurements also reveal that the v_1 slopes for the measured mesons become more negative as the collisions become more peripheral, which is consistent with the enhanced spectator shadowing effects observed in such events.

The results of the JAM model calculation in cascade mode, represented as blue solid lines in the figure, qualitatively describe the anti-flow at low p_T , even though the JAM model fails to reproduce the v_1 of kaons over the broad p_T range $0.4 - 1.6$ GeV/c, as shown in Fig. 2. Through a comparative analysis of the results with and without spectators, it is observed that the spectator shadowing effect induces a shift in the meson v_1 slope towards the negative direction. The JAM calculations for pions exhibit a similar dependence to that of the K_S^0 , and the v_1 slope of the pions is notably shifted further below zero at low p_T . This indicates that the spectator shadowing effect is responsible for the observed anti-flow at low p_T for both pions and kaons. To understand the kaon v_1 data in the high baryon density region, it is crucial to account for the spectator shadowing effect, which is a significant factor beyond the kaon potential.

In summary, we reported measurements of v_1 for π^\pm , K^\pm , K_S^0 , protons, and Λ in mid-central (10-40%) Au

+ Au collisions at $\sqrt{s_{\text{NN}}} = 3.0, 3.2, 3.5,$ and 3.9 GeV. The magnitude v_1 slopes of all above mentioned particles decrease in magnitude as collision energy increases. A strong p_T dependence is observed in the slopes of v_1 ($dv_1/dy|_{y=0}$) for both pions and kaons, where the slopes are negative at low p_T ($p_T \leq 0.6$ GeV/c) in all of these collisions. As mentioned in the introduction, the E895 experiment reported kaon anti-flow (quantified by measurements of sideward flow $\langle p_x \rangle$) in a similar low p_T region, which was attributed to a repulsive kaon potential. We applied the same p_T cut for measuring the sideward flow $\langle p_x \rangle$ of kaons and protons as was used in the E895 experiment at $\sqrt{s_{\text{NN}}} = 3.83$ GeV [35, 72]. The $\langle p_x \rangle$ flow of protons is consistent between the STAR and E895 experiments. However, the anti-flow of K_S^0 measured by STAR is a factor of eight smaller than that observed in the E895 experiment. Additionally, STAR measurements show negative mid-rapidity v_1 slopes at low p_T for the various kaon species.

In the hadronic transport model JAM, a baryonic mean field is essential to reproduce the observed mid-rapidity v_1 of protons and Λ baryons. Furthermore, JAM model calculations, considering both scenarios with and without spectators, show that the presence of spectators causes a shift in the v_1 slope of mesons toward the negative direction, even in the absence of a kaon potential. This suggests that the anti-flow of kaons could be due to the shadowing effect of spectators rather than being exclusively caused by the kaon potential. Our findings indicate that spectators contribute significantly to the observed anti-flow of kaons at low p_T in the high baryon density region of heavy-ion collisions.

We thank the RHIC Operations Group and SDCC at BNL, the NERSC Center at LBNL, and the Open Science Grid consortium for providing resources and support. This work was supported in part by the Office of Nuclear Physics within the U.S. DOE Office of Science, the U.S. National Science Foundation, National Natural Science Foundation of China, Chinese Academy of Science, the Ministry of Science and Technology of China and the Chinese Ministry of Education, NSTC Taipei, the National Research Foundation of Korea, Czech Science Foundation and Ministry of Education, Youth and Sports of the Czech Republic, Hungarian National Research, Development and Innovation Office, New National Excellency Programme of the Hungarian Ministry of Human Capacities, Department of Atomic Energy and Department of Science and Technology of the Government of India, the National Science Centre and WUT ID-UB of Poland, the Ministry of Science, Education and Sports of the Republic of Croatia, German Bundesministerium für Bildung, Wissenschaft, Forschung und Technologie (BMBF), Helmholtz Association, Ministry of Education, Culture, Sports, Science, and Technology (MEXT), Japan Society for the Promotion of Science (JSPS) and Agencia Nacional de Investigación y Desarrollo (ANID)

of Chile.

-
- [1] A. Bzdak, S. Esumi, V. Koch, J. Liao, M. Stephanov, and N. Xu, Phys. Rept. **853**, 1 (2020), arXiv:1906.00936 [nucl-th].
 - [2] X. Luo, S. Shi, N. Xu, and Y. Zhang, Particles **3**, 278 (2020), arXiv:2004.00789 [nucl-ex].
 - [3] J. Chen *et al.*, Nucl. Sci. Tech. **35**, 214 (2024), arXiv:2407.02935 [nucl-ex].
 - [4] M. S. Abdallah *et al.* (STAR), Phys. Lett. B **827**, 137003 (2022), arXiv:2108.00908 [nucl-ex].
 - [5] J. Randrup and J. Cleymans, Phys. Rev. C **74**, 047901 (2006), arXiv:hep-ph/0607065.
 - [6] J. Adam *et al.* (STAR), Phys. Rev. C **102**, 034909 (2020), arXiv:1906.03732 [nucl-ex].
 - [7] G. E. Brown and H. Bethe, Astrophys. J. **423**, 659 (1994).
 - [8] N. K. Glendenning and J. Schaffner-Bielich, Phys. Rev. C **60**, 025803 (1999), arXiv:astro-ph/9810290.
 - [9] D. Lonardoni, A. Lovato, S. Gandolfi, and F. Pederiva, Phys. Rev. Lett. **114**, 092301 (2015), arXiv:1407.4448 [nucl-th].
 - [10] D. Gerstung, N. Kaiser, and W. Weise, Eur. Phys. J. A **56**, 175 (2020), arXiv:2001.10563 [nucl-th].
 - [11] A. M. Poskanzer and S. A. Voloshin, Phys. Rev. C **58**, 1671 (1998), arXiv:nucl-ex/9805001.
 - [12] D. Teaney and L. Yan, Phys. Rev. C **83**, 064904 (2011), arXiv:1010.1876 [nucl-th].
 - [13] M. Luzum and J.-Y. Ollitrault, Phys. Rev. Lett. **106**, 102301 (2011), arXiv:1011.6361 [nucl-ex].
 - [14] C. M. Hung and E. V. Shuryak, Phys. Rev. Lett. **75**, 4003 (1995), arXiv:hep-ph/9412360.
 - [15] C. Gale, S. Jeon, B. Schenke, P. Tribedy, and R. Venugopalan, Phys. Rev. Lett. **110**, 012302 (2013), arXiv:1209.6330 [nucl-th].
 - [16] B. Schenke, S. Jeon, and C. Gale, Phys. Rev. Lett. **106**, 042301 (2011), arXiv:1009.3244 [hep-ph].
 - [17] B. Schenke, S. Jeon, and C. Gale, Phys. Rev. C **82**, 014903 (2010), arXiv:1004.1408 [hep-ph].
 - [18] S. Ryu, V. Jovic, and C. Shen, Phys. Rev. C **104**, 054908 (2021), arXiv:2106.08125 [nucl-th].
 - [19] Y. B. Ivanov and A. A. Soldatov, Phys. Rev. C **102**, 024916 (2020), arXiv:2004.05166 [nucl-th].
 - [20] N. S. Tsegelnik, E. E. Kolomeitsev, and V. Voronyuk, Phys. Rev. C **107**, 034906 (2023), arXiv:2211.09219 [nucl-th].
 - [21] P. Bozek and I. Wyskiel, Phys. Rev. C **81**, 054902 (2010), arXiv:1002.4999 [nucl-th].
 - [22] Y. Nara and A. Ohnishi, Phys. Rev. C **105**, 014911 (2022), arXiv:2109.07594 [nucl-th].
 - [23] D. H. Rischke, S. Bernard, and J. A. Maruhn, Nucl. Phys. A **595**, 346 (1995), arXiv:nucl-th/9504018.
 - [24] H. Stoecker, Nucl. Phys. A **750**, 121 (2005), arXiv:nucl-th/0406018.
 - [25] L. Adamczyk *et al.* (STAR), Phys. Rev. Lett. **112**, 162301 (2014), arXiv:1401.3043 [nucl-ex].
 - [26] L. Adamczyk *et al.* (STAR), Phys. Rev. Lett. **120**, 062301 (2018), arXiv:1708.07132 [hep-ex].
 - [27] J. Steinheimer, J. Auvinen, H. Petersen, M. Bleicher, and H. Stöcker, Phys. Rev. C **89**, 054913 (2014),

- arXiv:1402.7236 [nucl-th].
- [28] V. P. Konchakovski, W. Cassing, Y. B. Ivanov, and V. D. Toneev, *Phys. Rev. C* **90**, 014903 (2014), arXiv:1404.2765 [nucl-th].
 - [29] Y. Nara, H. Niemi, A. Ohnishi, and H. Stöcker, *Phys. Rev. C* **94**, 034906 (2016), arXiv:1601.07692 [hep-ph].
 - [30] A. Bialas and J. Czyzewski, *Phys. Lett. B* **222**, 132 (1989).
 - [31] H. Liu, S. Panitkin, and N. Xu, *Phys. Rev. C* **59**, 348 (1999), arXiv:nucl-th/9807021.
 - [32] H. Oeschler (KaoS), *Acta Phys. Polon. B* **29**, 3269 (1998).
 - [33] Z.-W. Lin, *Phys. Rev. C* **98**, 034908 (2018), arXiv:1704.08418 [nucl-th].
 - [34] C. Pinkenburg *et al.* (E895), *Phys. Rev. Lett.* **83**, 1295 (1999), arXiv:nucl-ex/9903010.
 - [35] P. Chung *et al.* (E895), *Phys. Rev. Lett.* **85**, 940 (2000), arXiv:nucl-ex/0101003.
 - [36] H. Liu *et al.* (E895), *Phys. Rev. Lett.* **84**, 5488 (2000), arXiv:nucl-ex/0005005.
 - [37] C. Zhang, J. Chen, X. Luo, F. Liu, and Y. Nara, *Phys. Rev. C* **97**, 064913 (2018), arXiv:1803.02053 [nucl-ex].
 - [38] Z. Liu, *EPJ Web Conf.* **296**, 05007 (2024), arXiv:2312.16758 [nucl-ex].
 - [39] Z.-W. Liu and S. Shi, *Phys. Rev. C* **110**, 034903 (2024), arXiv:2408.07563 [nucl-th].
 - [40] G.-Q. Li, C. M. Ko, and B.-A. Li, *Phys. Rev. Lett.* **74**, 235 (1995), arXiv:nucl-th/9410017.
 - [41] G. Q. Li and G. E. Brown, *Nucl. Phys. A* **636**, 487 (1998), arXiv:nucl-th/9804018.
 - [42] S. Pal, C. M. Ko, Z.-W. Lin, and B. Zhang, *Phys. Rev. C* **62**, 061903 (2000), arXiv:nucl-th/0009018.
 - [43] D. B. Kaplan and A. E. Nelson, *Phys. Lett. B* **175**, 57 (1986).
 - [44] G. E. Brown, C. M. Ko, Z. G. Wu, and L. H. Xia, *Phys. Rev. C* **43**, 1881 (1991).
 - [45] T. Waas, N. Kaiser, and W. Weise, *Phys. Lett. B* **379**, 34 (1996).
 - [46] J. Schaffner and I. N. Mishustin, *Phys. Rev. C* **53**, 1416 (1996), arXiv:nucl-th/9506011.
 - [47] M. Anderson *et al.*, *Nucl. Instrum. Meth. A* **499**, 659 (2003), arXiv:nucl-ex/0301015.
 - [48] K. H. Ackermann *et al.* (STAR), *Nucl. Instrum. Meth. A* **499**, 624 (2003).
 - [49] M. L. Miller, K. Reygers, S. J. Sanders, and P. Steinberg, *Ann. Rev. Nucl. Part. Sci.* **57**, 205 (2007), arXiv:nucl-ex/0701025.
 - [50] W. J. Llope *et al.*, *Nucl. Instrum. Meth. A* **522**, 252 (2004), arXiv:nucl-ex/0308022.
 - [51] A. Banerjee, I. Kisel, and M. Zyzak, *Int. J. Mod. Phys. A* **35**, 2043003 (2020).
 - [52] K. Wang, J. Zhou, X. Wang, X. Li, D. Hu, and Y. Sun, *Nucl. Instrum. Meth. A* **1057**, 168778 (2023).
 - [53] J. Adams *et al.*, *Nucl. Instrum. Meth. A* **968**, 163970 (2020), arXiv:1912.05243 [physics.ins-det].
 - [54] U. Gürsoy, D. Kharzeev, and K. Rajagopal, *Phys. Rev. C* **89**, 054905 (2014), arXiv:1401.3805 [hep-ph].
 - [55] U. Gürsoy, D. Kharzeev, E. Marcus, K. Rajagopal, and C. Shen, *Phys. Rev. C* **98**, 055201 (2018), arXiv:1806.05288 [hep-ph].
 - [56] A. I. Sheikh, D. Keane, and P. Tribedy, *Phys. Rev. C* **105**, 014912 (2022), arXiv:2110.04283 [nucl-ex].
 - [57] S. Chatterjee and P. Bozek, *Phys. Lett. B* **798**, 134955 (2019), arXiv:1804.04893 [nucl-th].
 - [58] L. Adamczyk *et al.* (STAR), *Phys. Rev. Lett.* **108**, 202301 (2012), arXiv:1112.3930 [nucl-ex].
 - [59] Y. Nara, N. Otuka, A. Ohnishi, K. Niita, and S. Chiba, *Phys. Rev. C* **61**, 024901 (2000), arXiv:nucl-th/9904059.
 - [60] Y. Nara, T. Maruyama, and H. Stoecker, *Phys. Rev. C* **102**, 024913 (2020), arXiv:2004.05550 [nucl-th].
 - [61] H. Sorge, *Phys. Rev. C* **52**, 3291 (1995), arXiv:nucl-th/9509007.
 - [62] Z.-W. Lin, C. M. Ko, B.-A. Li, B. Zhang, and S. Pal, *Phys. Rev. C* **72**, 064901 (2005), arXiv:nucl-th/0411110.
 - [63] K. Nayak, S. Shi, N. Xu, and Z.-W. Lin, *Phys. Rev. C* **100**, 054903 (2019), arXiv:1904.03863 [nucl-ex].
 - [64] W. Cassing and E. L. Bratkovskaya, *Nucl. Phys. A* **831**, 215 (2009), arXiv:0907.5331 [nucl-th].
 - [65] T. Hirano and Y. Nara, *PTEP* **2012**, 01A203 (2012), arXiv:1203.4418 [nucl-th].
 - [66] H. Sorge, H. Stoecker, and W. Greiner, *Annals Phys.* **192**, 266 (1989).
 - [67] S. A. Bass *et al.*, *Prog. Part. Nucl. Phys.* **41**, 255 (1998), arXiv:nucl-th/9803035.
 - [68] M. Bleicher *et al.*, *J. Phys. G* **25**, 1859 (1999), arXiv:hep-ph/9909407.
 - [69] M. S. Abdallah *et al.* (STAR), *Phys. Lett. B* **827**, 136941 (2022), arXiv:2112.04066 [nucl-ex].
 - [70] B. Aboona *et al.* (STAR), *Phys. Rev. Lett.* **130**, 212301 (2023), arXiv:2211.16981 [nucl-ex].
 - [71] R. J. M. Snellings, H. Sorge, S. A. Voloshin, F. Q. Wang, and N. Xu, *Phys. Rev. Lett.* **84**, 2803 (2000), arXiv:nucl-ex/9908001.
 - [72] C. Pinkenburg *et al.* (E895), *Nucl. Phys. A* **698**, 495 (2002), arXiv:nucl-ex/0104025.